Composite Structures 308 (2023) 116714

Contents lists available at ScienceDirect

Composite Structures

journal homepage: www.elsevier.com/locate/compstruct

A hybrid micro-macro mechanical damage model to consider the influence of resin-rich zones on the transverse tensile behaviour of unidirectional composites

M. Rezasefat [a], Y. Mostafavi [b], D. Ma [a], A. Manes [a,*]

[a] Politecnico di Milano, Dipartimento di Meccanica, via La Masa 1, Milano 20155, Italy
[b] Department of Civil and Environmental Engineering, University of Windsor, Windsor, Ontario, Canada

ARTICLE INFO

Keywords:
Hierarchical damage model
Composite failure
Puck failure criteria
Image processing
Fibre volume fraction

ABSTRACT

This paper presents a hierarchical hybrid micro-macro mechanical damage model aimed to simulate progressive failure in fibre reinforced composite materials. The hybrid model works based on performing image processing on the SEM cross-sectional images of microstructure to generate a location base file with the information of scattering of local volume fraction of the microstructure. The information is moved to a macro mechanical model which is implemented in Abaqus/Explicit using a user-defined material model. Prior to the macro mechanical analysis, the user-defined material model estimates the effective mechanical properties of each material point by using the local volume fraction and the analytical micromechanical models such as the rule of mixture, Chamis and Bridging. The hybrid damage model was verified by comparison with results from macroscale simulations with different fibre volume fractions. The hybrid model was used to analyze the resin-rich uncertainty in the composite material. The effect of the discretization window size was mitigated by using microstructure images and point-to-point mapping for the estimation of the mechanical properties. The presence of the resin-rich zone led to a 25.2 % decrease in the transverse stiffness and a 27.0 % increase in the failure strain which was well predicted by the hybrid model.

1. Introduction

The complex geometrical characteristic of unidirectional composites leads to a large number of uncertainty sources in turn leading to variability in the mechanical and thermal properties which can jeopardize the performance of composite components. The variations in microstructural morphologies such as fibre waviness, dry fibres, voids, resin-rich zones, and volume fraction variations introduce significant spatial scatter in composite stiffness and strength properties which are hard to predict due to batch-to-batch variability of test specimens. While studies of the effect of voids and fibre waviness in microstructures are abundant, the volume fraction variation and resin-rich zones are less discussed in the literature.

Fibre volume fraction variations and resin-rich areas or resin pockets are formed either due to scatter in permeability during the consolidation or impregnation phase of the manufacturing process or they are formed at the interface of laminae in the laminate as inter-laminar resin-rich layers. The presence of these resin-rich zones changes the local mechanical properties and failure mechanisms of the composite material [1]. Several researchers have tried to develop numerical models to include the influence of fibre volume variability and resin-rich areas. Microstructural Finite Element (FE) simulations of Fibre-Reinforced Polymer (FRP) by considering different constituents, i.e., fibres and matrix, have been proven to be accurate in predicting the mechanical response and failure [2,3]. Huang [4] presented a micromechanics damage model for the simulation of Unidirectional (UD) composites with different volume fractions. Using the information from composite constituents, i.e., fibres and resin, he managed to predict the tensile and shear behaviour of different composite materials. The effect of spatial arrangement and size of the resin-rich zone on mechanical responses was investigated by Ahmadian et al. [5]. By using statistical volume elements (SVE), they showed that the effect of the resin-rich zones is more severe under transverse compression load conditions compared to tensile loading conditions. Besides, it is uncovered that the presence of resin-rich zones leads to a decrease in the transverse tensile strength of the composite. Also on CFRP composites, Ghayoor et al. [6] studied the

* Corresponding author.
E-mail address: Andrea.manes@polimi.it (A. Manes).

https://doi.org/10.1016/j.compstruct.2023.116714
Received in revised form 22 December 2022; Accepted 14 January 2023
Available online 19 January 2023

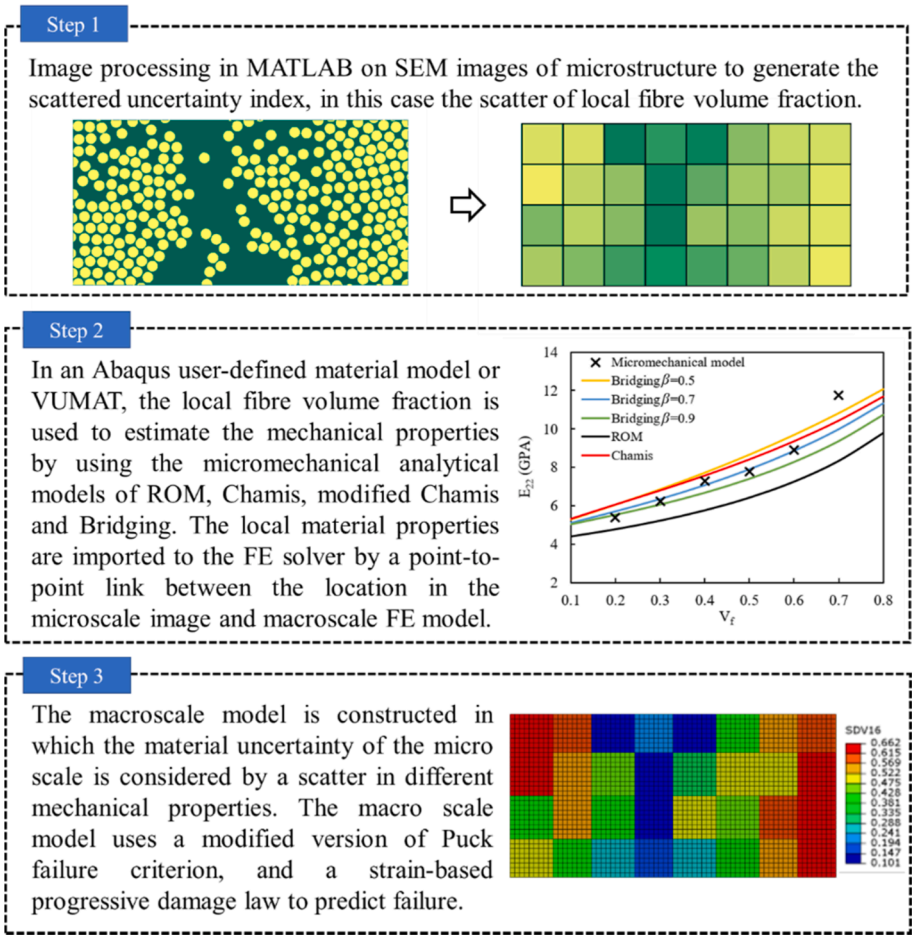

Fig. 1. The procedure of the hybrid micro-macro mechanical model.

effect of resin-rich pockets on the transverse properties. Representative volume elements (RVEs) with predefined resin pockets were used in finite element (FE) simulations to show that the resin pockets reduce the stiffness and failure strain of composite materials. More specifically, for samples with the same volume fractions, the ones with resin pockets fail at lower strains than the ones without. Jiang et al. [7] used micromechanical simulations to prove the possibility of improvements in elastic modulus and compressive strength of CFRP by using soft micro-length aramid pulp micro/nano-fibre interlays. The simulation results showed that the failure modes alterations benefit from using ultra-thin AP micro-fibre interlays leading to higher compressive strength.

FE simulations play an important role in the investigation of these issues. Yang et al. [8] investigated the influence of inter-fibre spacing on the transverse failure of composite using micromechanical FE simulations. A decrease in transverse properties was found in higher volume fractions and small inter-fibre spacing situations. Sharifpour et al. [1] performed micromechanical FE simulations to study the effect of manufacturing-induced defects such as fibre spatial distribution and microvoids on the tensile properties of cross-ply composite laminates. Due to a decrease in the distortion and dilatation energy levels, local yielding can be hindered in the resin-rich zone resulting in postponing the crack propagation once a crack reaches the resin-rich zone from adjacent fibre clusters. Jiang et al. [9] presented a microscale FE model to investigate the effect of voids on the mechanical properties and failure mechanisms of fibre bundles. The increase of void content resulted in a decrease in modulus and strength except for longitudinal properties where the presence of voids showed little influence.

Zhu et al. [10] developed a fatigue model to include the effect of random fibre distribution such as resin-rich zone and fibre clustering and observed that the presence of poorly distributed fibre zones has a significant effect on the fatigue life and location of the failure. Koley et al. [11] developed a numerical framework to study the effect of fibre volume variations inside an RVE on the effective elastic properties and observed that the fibre rich and resin-rich zones have a pivotal role in the prediction of the elastic properties of the RVE. Chu et al. [12] investigated the influence of defects such as voids on the elastic properties of composite materials by using micromechanical FE simulations and analytical approaches. It was reported that the analytical approaches can be considered effective in the prediction of the elastic properties of composite materials containing random void defects.

Sanei et al. [13] discussed the effectiveness of using RVE, SVE, and Uncorrelated Volume Element (UVE) in stochastic modelling of microstructure demonstrating that depending on the size and the location of the RVE, severe variation in the fibre volume fraction may exist. Therefore, the RVE cannot be an effective representative of the microstructure and does not include scatter because it does not allow variability. Meanwhile, the SVEs can be used for stochastic modelling since they allow the scatter, they need to be uncorrelated to be scattered randomly within the simulation domain. Sanei et al. [13] proposed a 70 μm window size to be the uncorrelated volume element for the random assignment of the properties.

In addition, multiscale approaches [14,15] have been widely applied in recent years to consider the effect of uncertainty in composite materials. Multiscale approaches allow micro/*meso* scale models to calculate equivalent material properties, which can be later used as the constitutive law in macroscale models [15,16]. Jiang et al. [17] presented a multiscale model to predict the shear strength and progressive damage of braided composites. Microscale representative unit cell was used to

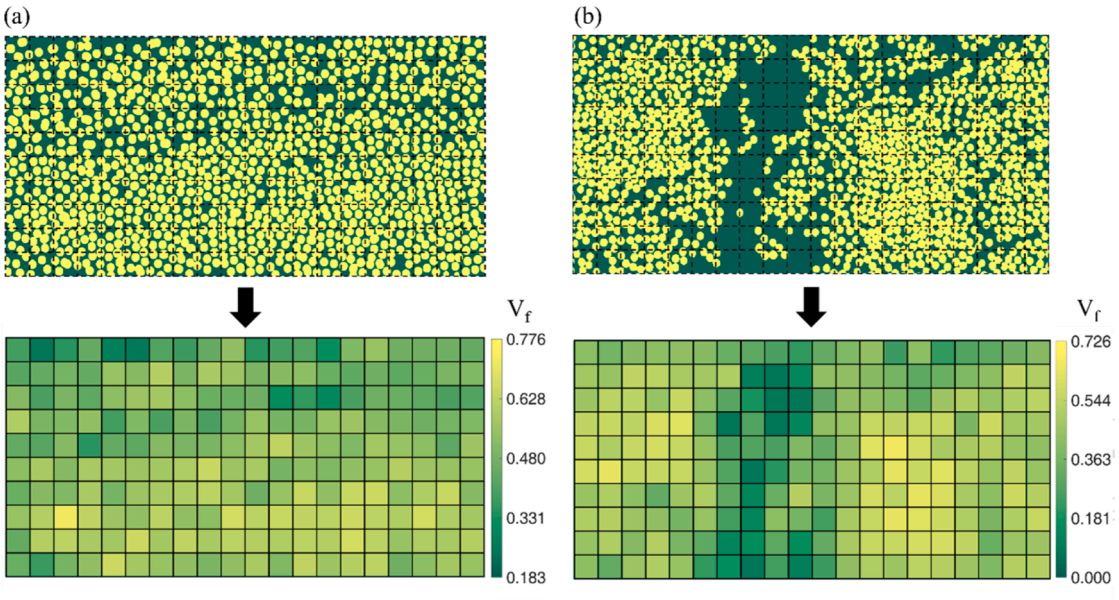

Fig. 2. Schematic view of the microstructure and its reconstruction using fibre volume-dependent elements, (a): Microstructure without resin-rich uncertainty, (b): Microstructure with resin-rich uncertainty. The microstructures have been processed based on the SEM image from [27,28].

calculate the effective properties that were later used to predict damage in a mesoscale model. The homogenization-based macroscale models can improve the efficiency of calculation, even for the cases of complex structures and/or loading conditions. More specifically regarding the investigation of uncertainty, it is found that the study based on meso-scale modelling is insufficient to evaluate the effect of uncertainty, while a larger scatter can be provided from the macroscale model compared with mesoscale ones [15,18]. Therefore, multi-scale approaches to consider the uncertainty of composite by doing simulations in both micro and macro models can lead to accurate results while complex modelling generation and high computational time are still a concern.

This work aims to present a non-stochastic hybrid micro and macroscale damage model to consider the effect of fibre volume variability and resin-rich zones in the prediction of transverse properties of FRP composites. An image-based reconstruction approach has been used here to assimilate the microstructure information by implementing analytical formulations to provide a point-to-point link between the microscale properties to the macro scale damage model. Several analytical micromechanical formulations such as the rule of mixture (ROM) [19], Chamis [20,21], modified Chamis [20,21] and Bridging [22,23] have been considered for the estimation of elastic and damage properties by using the information from the image processing on the microstructure. Using this approach, there is no need to perform FE simulations on the microstructure which makes the proposed model computationally effective. In order to consider the resin-rich uncertainties, the model should be capable of considering the variations of local fibre volume fractions in the microstructure. Accordingly, several RVEs of FRP microstructure with different volume fractions have been developed to calibrate the hybrid model. Finally, a block of microstructure with resin-rich uncertainty has been investigated using both the micromechanical model and the hybrid micro–macro scale model to investigate the capabilities of the hybrid model to predict of transverse properties of the microstructure with resin-rich uncertainty.

2. Methods

2.1. Description of the hybrid model

The hierarchical hybrid micro–macro mechanical model consists of three steps. First, the SEM cross-sectional microstructure image perpendicular to the fibre orientation is analyzed in an image-processing step in MATLAB in order to generate a topological file with the information on the scatter of the local volume fraction of the microstructure. The information is moved to the macro mechanical model which is implemented in Abaqus/Explicit using a user-defined material model or VUMAT. Prior to the macro mechanical analysis, a user-defined material model estimates the effective mechanical properties of each material point by using the local volume fraction and the analytical micromechanical models such as ROM, Chamis, modified Chamis and Bridging. The macroscale damage model incorporated the microstructure information by means of analytical formulations to estimate the elastic and damaged mechanical properties which depend on the local volume fraction in a non-stochastic manner. The macroscale damage step is based on the failure criterion of Puck [24,25] for initiation of inter-fibre fracture and a strain-based model to account for progressive failure, see Fig. 1 for the summarized procedure of the hybrid model. This section presents a detailed description of each step of the hybrid model. At the end of this section, the micromechanical FE models are described in which microstructure blocks of different fibre volume fractions are developed for the verification of the hybrid damage model.

2.2. The local fibre volume fraction

Local fibre volume fraction variation is one of the sources of microstructural variability in fibre-reinforced polymers. In many cases, an average fibre volume fraction is used in numerical simulations of fibre-reinforced polymers while a significant scatter in the local fibre volume fraction in different material locations is present. The changes in the local fibre volume fraction are the source of variation in stiffness and strength as well as fatigue properties. Image processing has been reported as a useful tool to quantify the local fibre volume fraction variability in an FRP microstructure. Here, similar to the approach of Sanei et al [13], the variation of local fibre volume fraction in different material points has been taken into account by partitioning the SEM image into a rectangular grid of square windows. It has been shown that the scatter in the local fibre volume fraction highly depends on the size of the window and that smaller window sizes lead to higher variations in the local fibre volume fraction. Most of the effort to determine the window size was put into finding the minimum RVE size to maintain the statistical homogeneity of the microstructure [13].

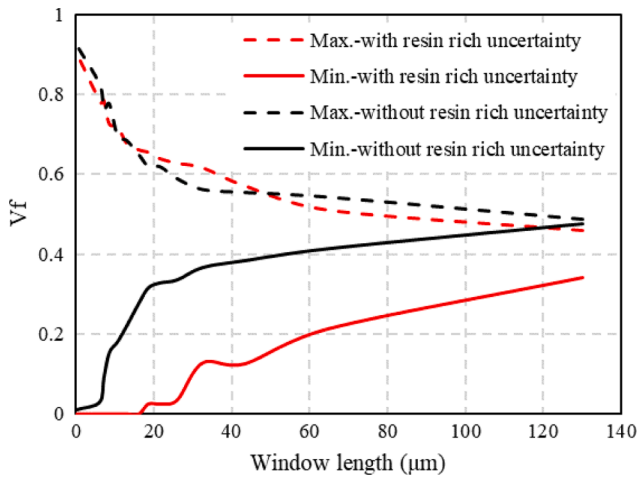

Fig. 3. The variation in local fibre volume fraction for the microstructure with and without resin-rich uncertainty with respect to the window length.

The image processing was performed in MATLAB to measure the fibre volume fraction in each window. For a clear distinction between the fibre and matrix in the SEM image, the intensity threshold and the edge detection methods have been used [26]. Due to the higher atomic number of fibres compared to the matrix, the fibres appear brighter in the SEM image which has been used to distinguish the fibre from the matrix. To better illustrate, the cross-section SEM images [27,28] of CFRP without and with resin-rich uncertainty were analyzed by image processing in Fig. 2-a and b, respectively. As can be seen the segmented image with square windows shows a scatter in the local fibre volume fraction which corresponds to the microstructure images of the CFRP. In each window, the local volume fraction has been calculated as the area of the volume of the fibres inside the window to the total window volume. The variation between the maximum and minimum value of scattered fibre volume fractions in each microstructure image depends on the segmentation window size. This variation has been shown in Fig. 3 for the two microstructures in Fig. 2. Higher variations can be obtained with a smaller window for the observation of both microstructures. Because decreasing the window size leads to the presence of several segmentation windows located in the resin-rich areas that determine the lower limit of the scattered volume fraction. Both the minimum and maximum value of the volume fraction in the microstructure without resin-rich uncertainty are susceptible to change with the change of the window size too, which is consistent with the conclusion of [13]. The relationship between the minimum and maximum volume fractions is different for the microstructure with the resin-rich uncertainty in comparison with the microstructure without

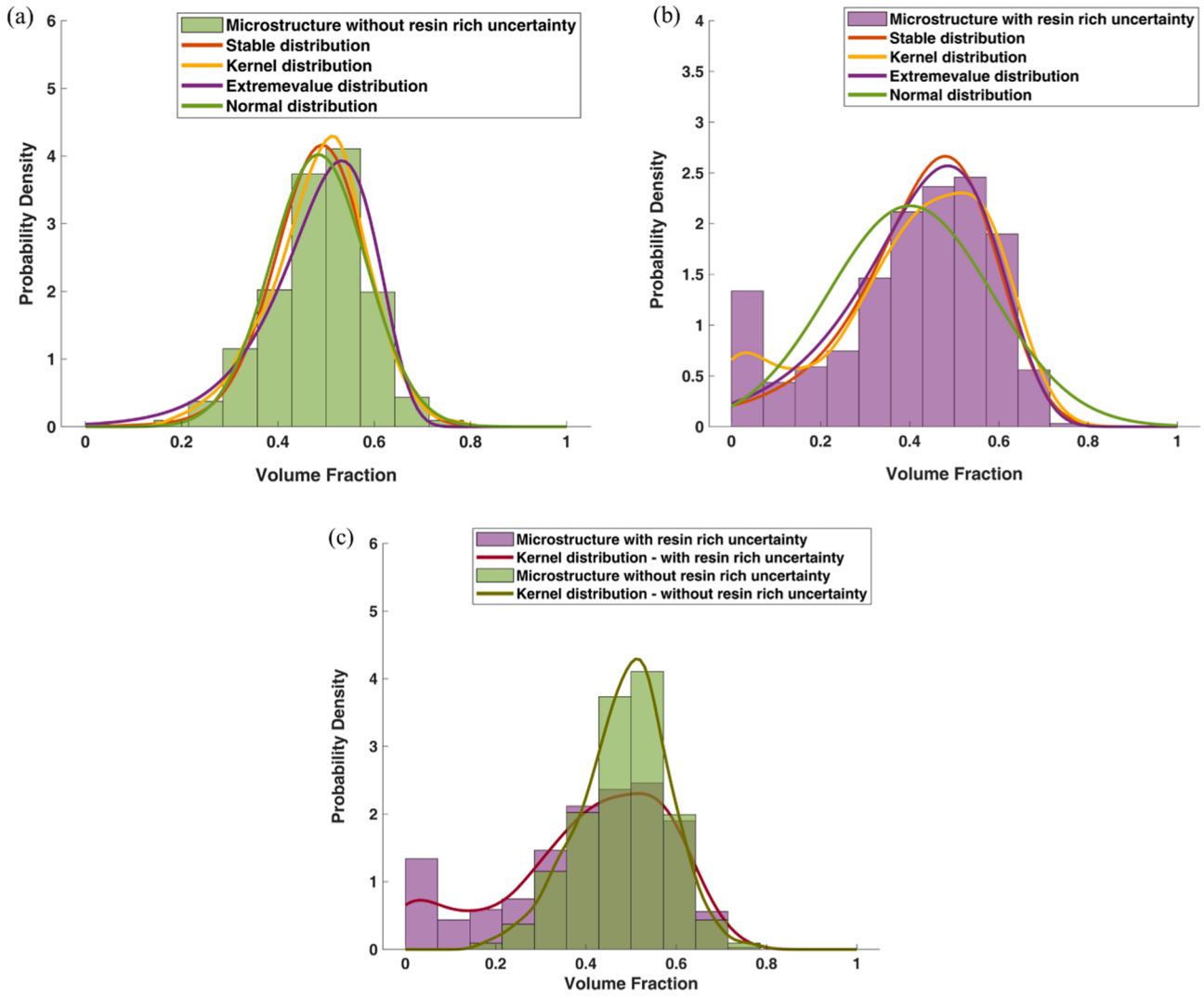

Fig. 4. Actual distribution and distribution fits of the local fibre volume fractions. (a): Microstructure without resin-rich uncertainty, (b): Microstructure with resin-rich uncertainty, (c): Comparison of both results.

resin-rich uncertainties; the minimum value of fibre volume fraction is significantly lower for all window sizes which is due to the presence of resin-rich zones. A further decrease in the window size leads to the minimum value of zero in the microstructure with resin-rich uncertainty that was not observed in the other microstructure. In addition, higher variations in all the different investigated window sizes have been observed for the microstructure with resin-rich uncertainty which is an important aspect in stochastic FE modelling of FRP with uncertainties and should be considered in simulations. More information on the proper window size for stochastic simulations can be found here [13].

To better illustrate the difference between the segmented representative elements of the microstructure with and without the resin-rich uncertainty, the volume fraction distributions for the microstructures in Fig. 2 have been compared in Fig. 4. From the comparison of Fig. 4-a and b it can be seen that the presence of resin-rich uncertainty has led to a significant increase in the probability density of the windows with low-volume fractions. In [13] several distribution fits, such as Weibull, Beta, and Extreme value were suggested to represent the actual distribution of the volume fraction variation. Whereas here better results were achieved using Kernel distribution. Fig. 4-c shows the comparison of the actual distribution of the fibre volume fraction for both microstructures with the Kernel fit. The Kernel distribution fit was accurate in representing the fibre volume fraction distribution of both microstructures. A discussion on the effect of the window size on the scatter of material properties and response of the FRP microstructures is presented in Section 3.3.

2.3. Analytical models for the estimation of mechanical properties

This section presents a brief description of the analytical homogenization models for the estimation of transverse elastic properties and transverse strength of unidirectional composites. Different analytical approaches have been presented for the elastic and strength properties among which the rule of mixture (ROM) [19], Bridging [22,23] and Charmis [20,21] models are considered for the estimation of effective elastic properties; while the Charmis model [20,21], modified Chamis model [20,21], and Bridging model [29] have been chosen for the estimation of transverse strength of FRP composite. The selection of the models was work based on the comparative studies performed in [30,31].

2.3.1. Elastic properties

- **Rule of mixture (ROM)**

The well-known rule of mixture model has been widely used for the estimation of material properties in fibrous composites. This model predicts the overall material properties in terms of the properties of the constituent phases with regard to their volume fraction. The ROM equation for the prediction of longitudinal young's modulus has been proven to be accurate, therefore the ROM, i.e., Equation (1) has been used for the estimation of the longitudinal young's modulus (E_{11}). The transverse young's modulus (E_{22}), Poisson's ratio (ν_{12}), and in-plane shear modulus (G_{12}) are estimated by Equations (2), (3), and (4) by the ROM method, respectively.

$$E_{11} = V_f E^f_{11} + V_m E^m \tag{1}$$

$$E_{22} = \frac{E^f_{22} E^m}{E^m V_f + E^f_{22} V_m} \tag{2}$$

$$\nu_{12} = V_f \nu^f_{11} + V_m \nu^m \tag{3}$$

$$G_{12} = \frac{G^f_{12} G^m}{G^m V_f + G^f_{12} V_m} \tag{4}$$

where V_f is the fibre volume fraction and V_m is the matrix volume fraction. The suffixes "m" and "f" refer to matrix and fibre, respectively used to express the properties of constituents.

- **Chamis model**

The semi-empirical micromechanical model of Chamis [20,21] expresses all the independent elastic properties with separate empirical equations except for the E_{11} and ν_{12} which are estimated with the ROM relations. The Chamis formulations for transverse elastic properties are as follows:

$$E_{22} = \frac{E^m}{1 - \sqrt{V_f}\left(1 - E^m / E^f_{22}\right)} \tag{5}$$

$$G_{12} = \frac{G^m}{1 - \sqrt{V_f}\left(1 - G^m / G^f_{12}\right)} \tag{6}$$

$$G_{23} = \frac{G^m}{1 - \sqrt{V_f}\left(1 - G^m / G^f_{23}\right)} \tag{7}$$

- **Bridging model**

The Bridging model has been proposed by Huang [22,23], which predicts the elastic properties according to the following equations:

$$E_{22} = \frac{(V_f + V_m a_{11})((V_f + V_m a_{22})}{(V_f + V_m a_{11})(V_f S^f_{22} + V_m a_{22} S^m_{22}) + V_f V_m (S^m_{21} - S^f_{21}) a_{12}} \tag{8}$$

$$G_{12} = \frac{(V_f + V_m a_{66})(G^f_{12} G^m)}{V_f G^m + V_m a_{66} G^f_{12}} \tag{9}$$

$$G_{23} = \frac{0.5(V_f + V_m a_{44})}{V_f (S^f_{22} - S^f_{23}) + V_m a_{44} (S^m_{22} - S^m_{23})} \tag{10}$$

In the above equations the a_{ij} are the bridging matrix components [22,23] and the S^k_{ij} are the components of the compliance matrices of the matrix and fibre for k = m and k = f, respectively.

2.3.2. Transverse strength

- **Chamis model**

By dividing the RVE into subregions and considering a square fibre packing array, Chamis developed [20,21] the Equations (11) and (12) for the prediction of transverse tensile (S^t_{22}) and shear strength (S^s_{12}) of fibrous composites, respectively.

$$S^t_{22} = \left[1 - \left(\sqrt{V_f} - V_f\right)\left(1 - \frac{E^m}{E^f_{22}}\right)\right] S^m_t \tag{11}$$

$$S^s_{12} = \left[1 - \left(\sqrt{V_f} - V_f\right)\left(1 - \frac{G^m}{G^f_{12}}\right)\right] S^m_s \tag{12}$$

where S^m_t, and S^m_s are the matrix tensile and shear strength, respectively.

- **Modified Chamis model**

By using the assumptions of the Chamis model and using Equation (11), a modified version of the Chamis equation has been presented (Equation (13)) which is reported to provide a more accurate estimation of the transverse tensile strength [31].

$$S^t_{22} = \left[1 - \left(\sqrt{V_f} - V_f\right)\left(1 - \frac{E^m}{E^f_{22}}\right)\right]^{n_t} S^m_t \tag{13}$$

where n_t is calibrated in Section 3.2.

- **Bridging model**

The transverse strength is estimated by Equation (14) in the bridging model [22,23,32] which considers the stress concentration in the vicinity of fibres in the microstructure.

$$S^t_{22} = \left[V_f \frac{E^f_{22}}{\left(\beta E^f_{22} + (1-\beta)E^m\right)} + \left(1 - V_f\right) \right] \frac{S^m_t}{K^t_{22}} \tag{14}$$

where β is the Bridging parameter discussed in Section 3, and K^t_{22} is the stress concentration factor and is calculated by Equation (15).

$$K_{22}(\varphi) = \left\{ 1 + \frac{a}{2}\sqrt{V_f}\cos(2\varphi) + \frac{b}{2\left(1-\sqrt{V_f}\right)}\left[V_f^2\cos(4\varphi) + 4(1-2\cos(2\varphi))V_f\cos^2(\varphi) + \sqrt{V_f}\left(2\cos(2\varphi)+\cos(4\varphi)\right)\right]\right\} \frac{V_f E^f_{22} + \left(1-V_f\right)\left[\beta E^f_{22} + (1-\beta)E^m\right]}{\beta E^f_{22} + (1-\beta)E^m} \tag{15}$$

where $\phi = \frac{\pi}{4} + \frac{1}{2}\text{asin}\left(\frac{S^m_c - S^m_t}{S^m_c + S^m_t}\right)$ and for the transverse tensile the stress concentration factor is given as:

$$K^t_{22} = K_{22}(0) \tag{16}$$

While:

$$a = \frac{\left[1 - \nu^m - 2(\nu^m)^2\right]E^f_{22} - \left[1 - \nu^f_{23} - 2\left(\nu^f_{23}\right)^2\right]E^m}{(1+\nu^m)E^f_{22} + \left[1 - \nu^f_{23} - 2\left(\nu^f_{23}\right)^2\right]E^m} \tag{17}$$

$$b = \frac{\left(1+\nu^f_{23}\right)E^m - (1+\nu^m)E^f_{22}}{\left[\nu^m + 4(\nu^m)^2 - 3\right]E^f_{22} - \left(1+\nu^f_{23}\right)E^m} \tag{18}$$

2.4. Macro mechanical constitutive and damage model

The macro-homogeneous simulation of composites is preferred over the micromechanical method in many situations due to computational limitations [33]. Instead of considering all the constituents of the composite material, the global behaviour of lamina is described by the macro-homogeneous simulation. The Continuum Damage Mechanics (CDM) approach at the macro level has been used for FE simulations of progressive damage in composites based on the previous work presented in [34]. The progressive failure of composites is based on selectively degrading the stiffness parameters of the material. The degradation of stiffness parameters is controlled by damage variables which are the output of a linear strain-based damage evolution law. By defining different variables, only stiffness parameters corresponding to the failure mode of the material are degraded.

The inter-fibre failure criterion of Puck [24,25] for unidirectional composites has been used here. The failure criterion of Puck consists of two equations to calculate the material exposure in tension ($\sigma_n(\theta) > 0$) and compression ($\sigma_n(\theta) < 0$), i.e., *IFF1* and *IFF2* of Equation (19). The material exposure ranges from 0 to 1 where 0 means the unload condition and 1 indicates the onset of damage.

Table 1
Mechanical properties for the micromechanical simulation.

Mechanical property	Notation	Value
Longitudinal modulus	E_{11}(GPa)	Equation (1)
Transverse modulus	E_{22}(GPa)	Equation (2), (5), and (8)
Through-thickness modulus	E_{33}(GPa)	Equation (2), (5), and (8)
In-plane shear modulus	G_{12}(GPa)	Equation (4), (6), and (9)
Transverse shear modulus	G_{13}(GPa)	Equation (4), (6), and (9)
Through-thickness shear modulus	G_{23}(GPa)	Equation (7)
Major Poisson's ratio	ν_{12}	Equation (3)
Major transverse Poisson's ratio	ν_{13}	Equation (3)
Through thickness Poisson's ratio	ν_{23}	0.49
Transverse tensile strength	S^t_{22}(MPa)	Equation (11), (13), and (14)
In-plane shear strength	S^s_{12}(MPa)	Equation (12)

$$f_{e1}(\theta) = \sqrt{\left[\left(\frac{1}{R^t_\perp} - \frac{P^t_{\perp\Psi}}{R^A_{\perp\Psi}}\right)\sigma_n\right]^2 + \left(\frac{\tau_{nt}}{R^A_{\perp\perp}}\right)^2 + \left(\frac{\tau_{nl}}{R^A_{\perp\parallel}}\right)^2} + \frac{P^t_{\perp\Psi}}{R^A_{\perp\Psi}}\sigma_n \quad for \quad \sigma_n \geq 0$$

$$f_{e2}(\theta) = \sqrt{\left(\frac{\tau_{nt}}{R^A_{\perp\perp}}\right)^2 + \left(\frac{\tau_{nl}}{R^A_{\perp\parallel}}\right)^2 + \left(\frac{P^c_{\perp\Psi}}{R^A_{\perp\Psi}}\sigma_n\right)^2} + \frac{P^c_{\perp\Psi}}{R^A_{\perp\Psi}}\sigma_n \quad for \quad \sigma_n < 0 \tag{19}$$

In the above equation we have:

$$\frac{P^t_{\perp\Psi}}{R^A_{\perp\Psi}} = \frac{P^t_{\perp\perp}}{R^A_{\perp\perp}}cos^2\Psi + \frac{P^t_{\perp\parallel}}{R^A_{\perp\parallel}}sin^2\Psi \tag{20}$$

$$\frac{P^c_{\perp\Psi}}{R^A_{\perp\Psi}} = \frac{P^c_{\perp\perp}}{R^A_{\perp\perp}}cos^2\Psi + \frac{P^c_{\perp\parallel}}{R^A_{\perp\parallel}}sin^2\Psi \tag{21}$$

while:

$$cos^2\Psi = 1 - sin^2\Psi = \frac{\tau^2_{nt}}{\tau^2_{nt} + \tau^2_{nl}} \tag{22}$$

$$R^A_{\perp\perp} = \frac{R^c_\perp}{2\left(1 + P^c_{\perp\perp}\right)} \tag{23}$$

where according to [24] $R^t_\perp = S^t_{22}$, and $R^A_{\perp\parallel} = S^s_{12}$ are the normal and shear strengths, respectively. Also, $P^t_{\perp\perp}$, $P^t_{\perp\parallel}$, $P^c_{\perp\perp}$, and $P^c_{\perp\parallel}$ are inclination parameters to describe the master fracture body and the material strengths are expressed in the action plane. On criticality of the inter fibre failure criterion of Puck is the need for a search algorithm to find the fracture angle orientation which adds a significant computational cost to the FE solution. Here the Simple Parabolic Interpolation Search (SPIS) [34] has been used to estimate the fracture angle orientation for each element during the explicit simulation. SPIS is a non-iterative algorithm to estimate the maximum exposure functions of Equation (19) and operates by isolating the ranges that potentially contain the global maxima in the exposure curve. More information on the SPIS can be

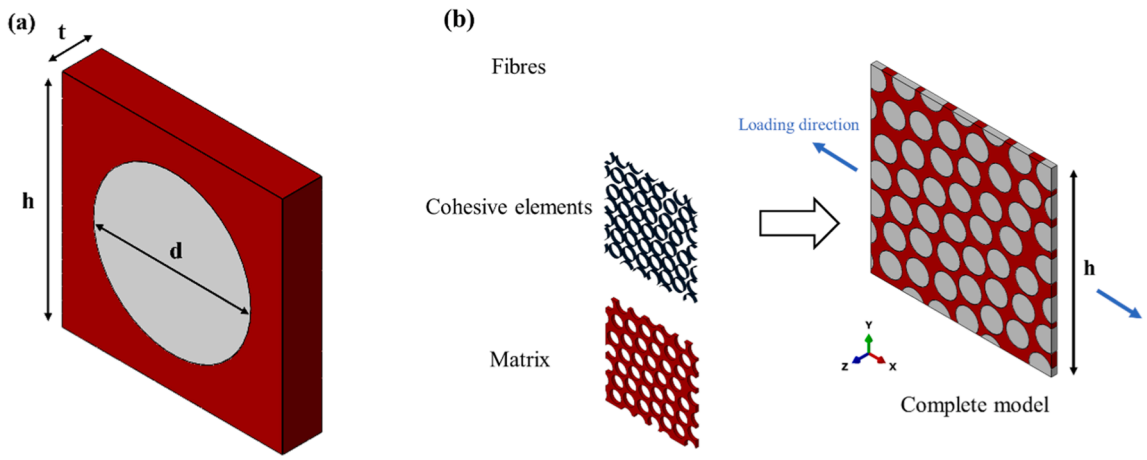

Fig. 5. Microstructure FE models, (a): Single fibre models, (b): The model with 50 fibres and its constituents including fibres, matrix and zero thickness cohesive elements.

found here [34].

The damaged stiffness matrix is achieved by selectively degrading the stiffness parameters the damage parameter d_m see [34] for more information. Since the transverse properties are of interest here, the fibre direction failure modes were ignored and the material properties corresponding to the fibre direction remain untouched during the simulations. The damage parameters d_m is a damage variable for matrix and matrix-shear failure. The damage parameter is measured according to Equation (24).

$$d_m = (1 - d_{IFF1})(1 - d_{IFF2}) \tag{24}$$

In Equation (24) the d_{IFF1} and d_{IFF2} are the damage indices for the tensile and compression failure modes of Puck failure criteria, respectively. Once the failure criteria of Equation (19) are met, the damage indices increase from zero according to the strain-based progressive damage model of Equation (25).

$$d_i = \frac{\varepsilon_{i,u}}{\varepsilon_{i,u} - \varepsilon_{i,on}}\left(1 - \frac{\varepsilon_{i,on}}{\varepsilon_i}\right) \tag{25}$$

In the above equation, the subindex i represents different failure modes of Equation (19). $\varepsilon_{i,u}$ represents the ultimate failure strain which depends on element characteristic length and fracture energy to avoid strain localization. The ε_i is the equivalent strain and is equal to $\sqrt{\langle \varepsilon_n \rangle^2 + {\gamma_{nt}}^2 + {\gamma_{nl}}^2}$ for tension and compression. In addition, $\varepsilon_{i,on}$ is the failure onset strain for each failure mode and is equal to the equivalent strain of the onset of damage which is calculated only if the failure criteria are met.

The mechanical properties of the macro mechanical model are summarized in Table 1. As mentioned in Section 2.1, the volume fractions from image processing and the analytical micromechanics formulations in Section 2.3 are used to estimate the mechanical properties of the material for the micro-homogeneous simulations.

2.5. Micromechanics FE model

In this paper, micromechanical FE models have been used for the calibration and verification of the hybrid damage model. Several RVE models with a range of fibre volume content have been created to carry out the micromechanical FE analysis. Micromechanical models have been used for the prediction of transverse mechanical properties of the composition of fibres which are randomly distributed in the matrix domain based on the simulation approach presented by Naya et al [35]. The microstructure is assumed as a set of parallel fibres with a perfect circular shape that is randomly scattered in the polymer matrix. To guarantee that the fibre placement in the RVE is representative of the actual fibre placement in a composite ply, the fibre distribution in each RVE was developed by mimicking the fibre distribution of micrograph pictures of composite ply from [28]. In all of the micromechanical models, the carbon fibres were considered perfectly cylindrical with a diameter of 6.6 μm [36,37].

Table 2
Properties of carbon fibre and epoxy matrix used for microstructure FE simulation [39–41].

Mechanical property	Carbon fibre	Epoxy matrix
Elastic modulus in longitudinal direction-E_{11} (GPa)	238	4.08
Elastic modulus in transverse direction-E_{22} (GPa)	28	–
Poisson's ratio	0.28	0.38
Shear modulus-G_{12} (GPa)	24	–
Shear modulus-G_{23} (GPa)	7.2	–
Tensile yield stress (MPa)	–	99
Energy dissipation (J/m^2)	–	100
Internal friction angle-β		29

Three levels of micromechanical study were performed aiming to produce useful information on the transverse mechanical properties of composite material for the calibration of the hybrid damage model and to investigate the effectiveness of the hybrid model in the prediction of stress–strain response of composite with resin-rich uncertainty. To achieve this, initially, the single-fibre RVEs with different fibre volume fractions were analyzed. The representative RVE must contain an adequate number of fibres [35,37] to be reliable in capturing the key characteristics of composite microstructure. Approximately 50 fibres are sufficient in an RVE to achieve a good balance between accuracy and computational time [35]. To study the effect of the volume fraction, different RVEs must be generated with different fibre volume fractions which can be achieved by reducing the number of fibres in the domain or by increasing the size of the RVE. The latter option was used to be sure that the shape diameter and the total number of fibres are constant for different volume fractions. The changes in the volume fraction were implemented by increasing the size of the RVE and keeping the relative location of fibres the same in different models. Therefore, the generated RVE models had different lengths and widths while in all of them the thickness was equal to 1.65 μm [37]. Finally, one block of microstructure was developed to investigate the resin-rich uncertainty in the CFRP composite. The shape and size of the resin-rich uncertainty have been defined by replicating an SEM image of a composite with such uncertainty from [38]. Examples of micromechanical FE models have been shown in Fig. 5-a and b for RVE with one and 50 fibres, respectively.

In all these models the perfectly circular and transversely isotropic carbon fibres are models as linear elastic solids and are constituted by

Table 3
Summary of FE models.

Model	Volume fraction	h (μm)	Micromechanical FE model		Hybrid model
			N. of solid elements	N. of cohesive elements	N. of solid elements
Single fibre	0.20	13.1	2502	126	1
	0.30	10.7	1689	126	1
	0.40	9.2	1341	126	1
	0.50	8.3	1137	126	1
	0.60	7.6	954	126	1
	0.70	7.0	855	126	1
50 fibres	0.31	72	443,340	19,116	324
	0.42	62	328,782	19,056	256
	0.60	52	235,896	18,786	169
	0.70	46	187,884	18,048	144

five elastic and independent constants of E_{f1}, E_{f2}, ν_{f12}, G_{f12}, and G_{f23}. The elastoplastic polymer matrix was simulated with a damage plasticity model which is accurate in the simulation of the polymer matrix [35]. The isotropic polymer matrix is described with two constants of elastic modulus and Poisson ratio, i.e., E_m and ν_m in the elastic region.

A modified Drucker-Prager plasticity yield surface is defined in the damage plasticity model with two damage indices to account for the quasi-brittle behaviour of the material in compressive and tension-dominant loading cases, for more information on the model see [35]. The mechanical properties used for the micromechanical FE simulations are presented in Table 2.

The debonding between the matrix and fibre was simulated by means of zero thickness cohesive elements. The fibre/matrix interface properties were chosen based on the parametric study performed in [37]. The bi-linear quadradic equation of (26) was used to account for the onset of the debonding in which only the tensile normal traction contributes to the onset of failure. Since the simulations were performed in the transverse direction, the mode I failure strength and fracture energy had a meaningful influence on the results. The mode I failure strength (σ_n^0) of 57 MPa and Mode II/III (τ_T^0 and τ_L^0) failure strength of 96 MPa were used here [37].

$$\left(\frac{\langle\sigma_n\rangle}{\sigma_n^0}\right)^2+\left(\frac{\tau_T}{\tau_T^0}\right)^2+\left(\frac{\tau_L}{\tau_L^0}\right)^2=1 \tag{26}$$

Interface damage evolution follows the mixed-mode fracture energy laws of Benzeggagh and Kenane (B-K) [42], see Equation (27). Mode I and II interface fracture energy were set equal to 0.002 and 0.107 N/mm according to [37].

$$G_n^C+\left(G_s^C-G_n^C\right)\left\{\frac{G_S}{G_T}\right\}^{\eta}=G^C \tag{27}$$

where η is the B-K material constant and G_n^C,G_s^C are the critical normal fracture energy and critical shear fracture energy, respectively. Also, G_S and G_T are the out-of-plane and total dissipated energies.

3. Results and discussion

In this section, first, the transverse behaviour of the hybrid damage model is calibrated by comparison of the results from micromechanical FE simulations and the results from the hybrid damage model. A comparison is performed from the hybrid damage model with the use of different equations in Section 2.3 to investigate the capability of analytical and semi-analytical micromechanical models in the estimation of the material properties of the composite. In addition, the micromechanical FE model is validated by comparison with the experimental data at a fibre volume fraction of 0.6. The validity of the micromechanical model is verified by developing a model with approximately 50 fibres and comparing it with the experimental data. This is a crucial step since the result from the micromechanical FE models have been used to investigate the accuracy of the hybrid damage model. Finally, the hybrid damage model has been used for the simulation of a block of microstructure with resin-rich uncertainty. In each subsection, the results of both numerical approaches are presented and discussed.

3.1. RVE with a single fibre

Fig. 5-a shows the schematic of single fibre CFRP micromechanical FE models. The single fibre models have volume fractions in the range of 0.2 to 0.7. For the micromechanical FE simulations, the single fibre RVEs were discretized with a different number of elements depending on the total size of the RVE for the micromechanical simulations, see Table 3. While only a single element was used to discretize each model in simulations with the hybrid damage model. The predicted transverse stiffness and strength by the micromechanical model were used for the benchmarking of the hybrid damage model in terms of equations of Section 2.3 that were used within the model for the prediction of stiffness and strength of the homogenized composite.

The ROM formulation is sufficiently accurate in the estimation of the

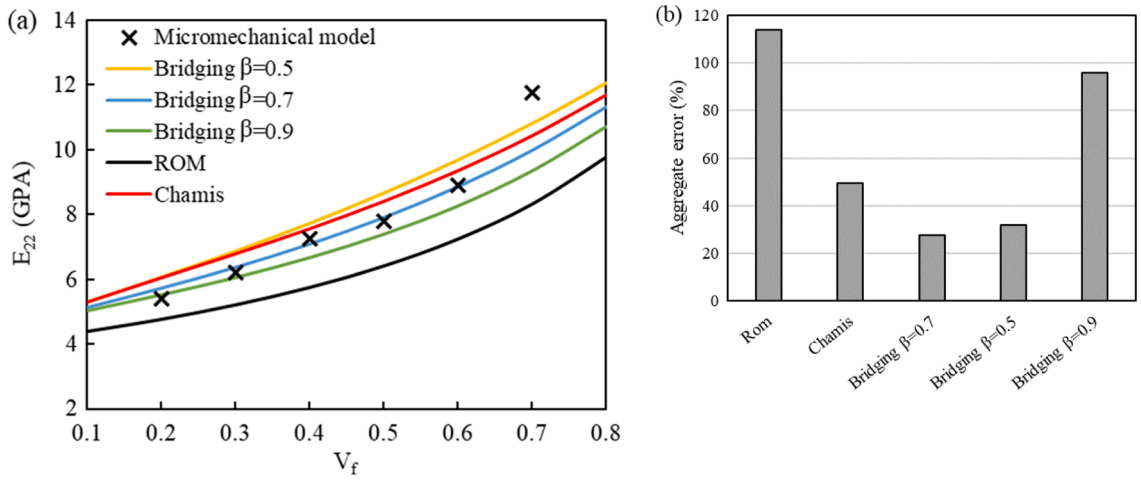

Fig. 6. Predicted transverse moduli of UD composite versus volume fraction. (a): The results of micromechanical formulations for the estimation of transverse moduli are also compared with the results of micromechanical FE simulation, (b): The aggregate error of each micromechanical formulation with respect to the micromechanical FE simulation.

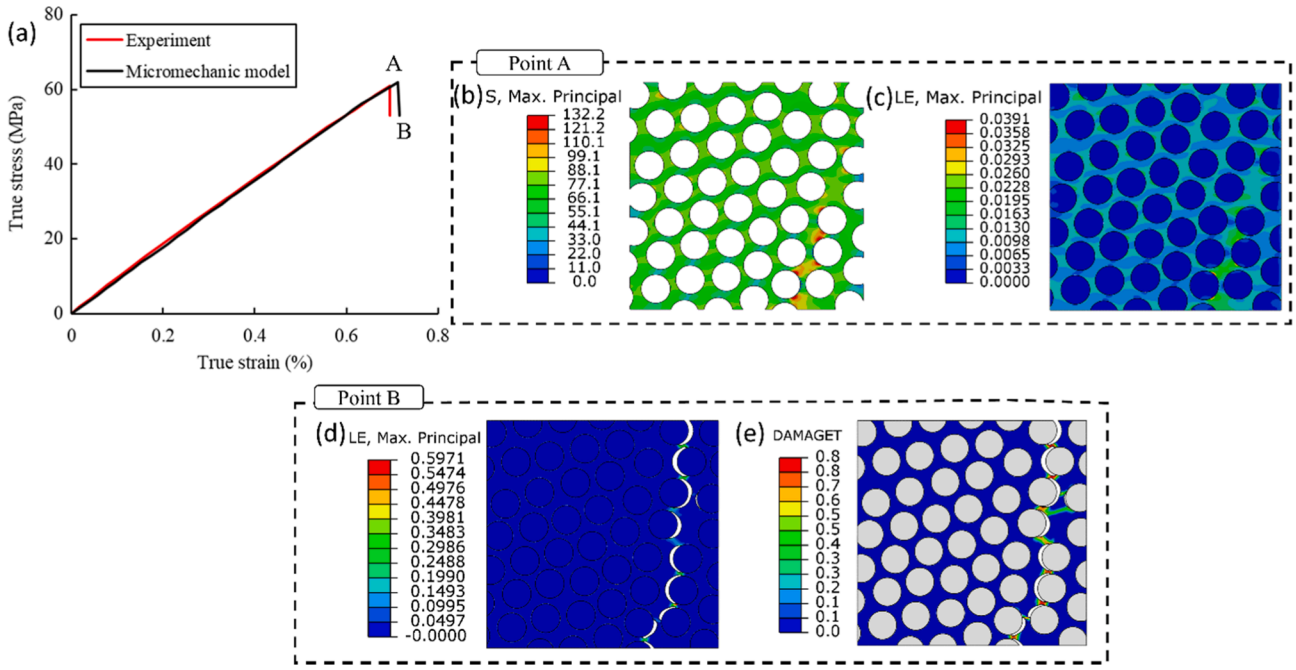

Fig. 7. The results of the micromechanical model with Vf = 0.6, (a): comparison of experimental and numerical stress–strain curves, (b and c): Distribution of stress and strain at Point A of the curve, respectively, (d and e): Distribution of strain and accumulative damage after the failure of the RVE, respectively.

longitudinal modulus and Poisson's ratio ν_{12} [4,43] of composite materials and is less sensitive to in-situ conditions compared to transverse properties. Therefore, ROM mixture equations of (1) and (3) have been used for the estimation of these properties in the hybrid damage model. The effective transverse properties are more sensitive to geometrical and manufacturing uncertainties such as perfect matrix/fibre bonding, faults and voids, volume fraction variation, etc. Consequently, a semi-analytical formulation has been developed to reach a better prediction of the transverse properties. Several works have compared the effectiveness of different micromechanics formulations for the prediction of effective material properties [31]. Here, as mentioned in Section 2.3, the ROM, the Chamis model formula and the Bridging model formula are considered for the elastic modulus in the transverse direction and the Chamis model, Modified Chamis and Bridging have been compared for the transverse strength to pick the best choice for the hybrid damage model.

Fig. 6-a and b show the prediction of transverse modulus by the ROM, Chamis, and Bridging model with different bridging parameters (β) which are compared with the results of the micromechanical FE simulation for single fibre models of different volume fractions. The ROM formulation underestimates the transverse stiffness of the composites, while a slight overestimation can be also observed from the results of the Chamis model formula. The bridging parameter (β) has been used here for the calibration of the Bridging model. It can be seen that using a smaller bridging parameter leads to a stiffer transverse modulus. Bridging parameters 0.5, 0.7 and 0.9 were examined to have a better fit with the experimental data, and here the transverse modulus calculated with $\beta = 0.7$ led to better agreement with the results of the micromechanical FE analysis for a single fibre RVE.

Therefore, the bridging parameters equal to 0.7 was the best option for the hybrid damage model. The single-fibre RVE has proven to be accurate in predicting the transverse modulus of the composite material to some extent. A percentage difference of 14 in the prediction of transverse modulus with respect to the experimental data has been reported in [11] which is a considerably large error and can be attributed to the primitive definition of fibre/matrix interface in the micromechanical model of [11]. While here a percentage difference of 1.6 % for the predicted transverse modulus with respect to the experimental data of [39] has been observed. The single fibre RVEs were not investigated for the relationship between the transverse strength and fibre volume fraction due to the complexity of the interaction between the epoxy matrix and fibre/matrix interface during the initiation and evolution of damage which was not present in the single fibre RVEs.

3.2. RVE with fifty fibres

In this section, first, the validity of the micromechanical FE model under pure transverse loading is assessed by comparison with existing micromechanical stress–strain experimental data of IM7/8552 UD carbon–epoxy composite with a volume fraction of 0.6 [37,39]. Then, the results of the micromechanical FE simulations of RVEs of different fibre volume fractions have been used to evaluate the predictions of the transverse properties by the hybrid damage model.

In order to point out the validity of the micromechanical FE simulation, the comparison between the experimental and numerical stress–strain curves is shown in Fig. 7-a for a microstructure with 50 fibres and a volume fraction of 0.6. It can be observed that the numerical result is in good agreement with the experimental data in the prediction of the stiffness and the transverse strength of the RVE. When subjected to pure transverse loading, the failure in the RVE is steered by the debonding at the fibre and matrix interface. The cracks that start at the interface cause the matrix/fibre debonding and this debonding leads to severe plastic deformation and the accumulation of matrix damage in the damaged zone. The stress concentration in the matrix at the onset of failure is shown by the maximum principal stress contour plot in Fig. 7-b. Fig. 7-c and d show the maximum principal strain contours at the corresponding displacements of A of Fig. 7-a and complete failure of the RVE, respectively. The plastic strain localization in the matrix in the vicinity of the interface debonding is well predicted by the numerical model. For pure transverse loading, the interface failure and matrix damage produce a failure path perpendicular to the loading direction, see Fig. 7-e. It is understood that the transverse tensile strength is ruled by the strength of the matrix/fibre interface [35,37]. Since the objective of the micromechanical FE simulations was to calibrate and investigate the accuracy of the hybrid damage models, the results of the micromechanical FE simulations are not presented in detail hereafter.

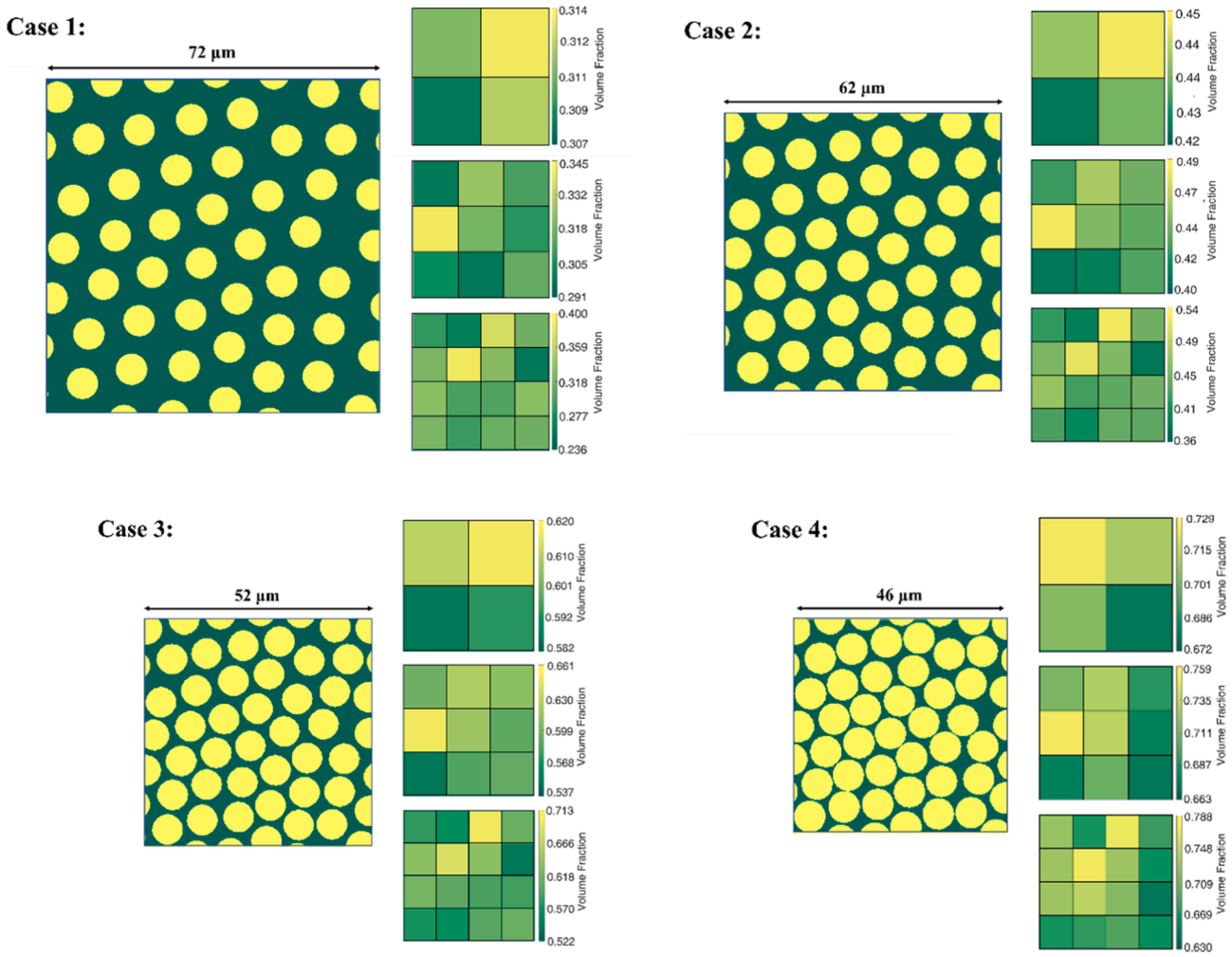

Fig. 8. Generated composite microstructures with different fibre volume fractions on the left with their discretization into 2 by 2, 3 by 3, and 4 by 4 window sizes on the right, (a): Case-1 with $V_f = 0.31$, (b): Case-2 with $V_f = 0.42$, (c): Case-3 with $V_f = 0.60$, (d): Case-4 with $V_f = 0.70$.

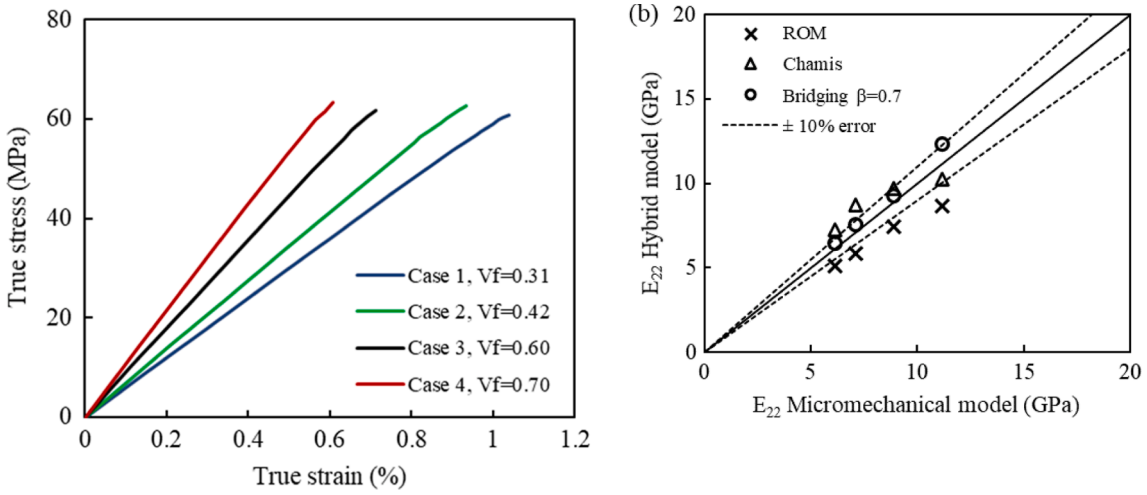

Fig. 9. (a): True stress–strain curves of the microstructure of Fig. 8 which are calculated by micromechanical FE simulation, (b): Comparison of the transverse stiffness estimated by the micromechanical model and the hybrid damage model.

Table 4
The estimation of the transverse modulus by ROM, Chamis, and Bridging formylations for the RVEs with 50 fibres and different total volume fractions.

Model	V_f	$E_{22}(GPa)$						
		Micromechanical FE model	Hybrid model with windows of:					
			2 × 2	Deviation (%)	3 × 3	Deviation (%)	4 × 4	Deviation (%)
ROM	0.31	6.15	5.11	−16.91	5.02	−18.37	5.08	−17.40
	0.42	7.12	5.82	−18.25	5.79	−18.68	5.91	−16.99
	0.60	8.89	7.45	−16.19	7.36	−17.21	7.39	−16.87
	0.70	11.17	8.63	−22.74	8.75	−21.66	8.73	−21.84
Chamis	0.31	6.15	7.26	18.05	7.19	16.91	7.2	17.07
	0.42	7.12	8.74	22.75	8.83	24.02	8.76	23.03
	0.60	8.89	9.71	9.22	9.78	10.01	9.74	9.56
	0.70	11.17	10.26	−8.15	10.44	−6.538	10.77	−3.58
Bridging	0.31	6.15	6.43	4.55	6.42	4.39	6.43	4.55
	0.42	7.12	7.55	6.04	7.76	8.99	7.69	8.01
	0.60	8.89	9.27	4.27	9.17	3.15	9.22	3.71
	0.70	11.17	12.33	10.38	12.57	12.53	12.54	12.26

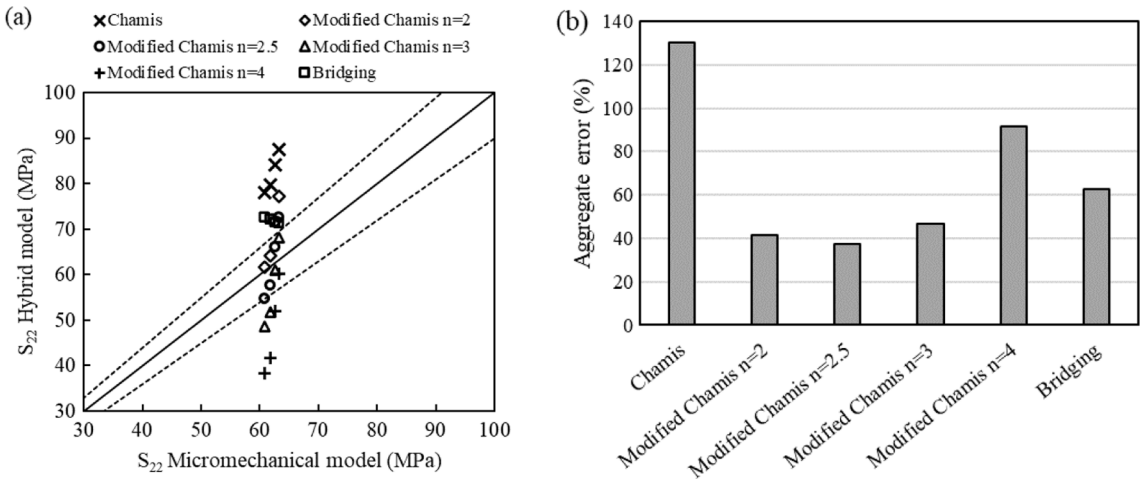

Fig. 10. (a): Comparison of the transverse strength estimated by the micromechanical model and the hybrid damage model, (b): The aggregate error of the hybrid model equipped with different analytical formulations for estimation of transverse strength.

The 50 fibre microstructures of different volume fractions are simulated by both the micromechanical FE and the hybrid damage model approaches. In the hybrid simulations, the RVE was studied with user-defined material models which were equipped with different analytical and semi-analytical formulations to estimate the mechanical properties. See Table 3 for more details on the models and Table 2 for a summary of the formulations to estimate the mechanical properties. Fig. 8 shows the reconstruction of the microstructure by using the image processing technique and the discretization method discussed in Section 2.2. In this figure, the light-yellow colour indicates the location of fibres while the epoxy matrix is coloured green. The local fibre volume variation is compared for 2 by 2, 3 by 3, and 4 by 4 window sizes for each of the microstructures of different total fibre volume fractions.

The microstructures of Fig. 8 have the total fibre volume fractions of 0.31, 0.42, 0.60, and 0.70 for Case-1, Case-2, Case-3, and Case-4, respectively. The scatter of the fibre volume variation is qualified by the window size, having a bigger range for smaller window sizes of the same microstructure. A significant scatter in the local fibre volume

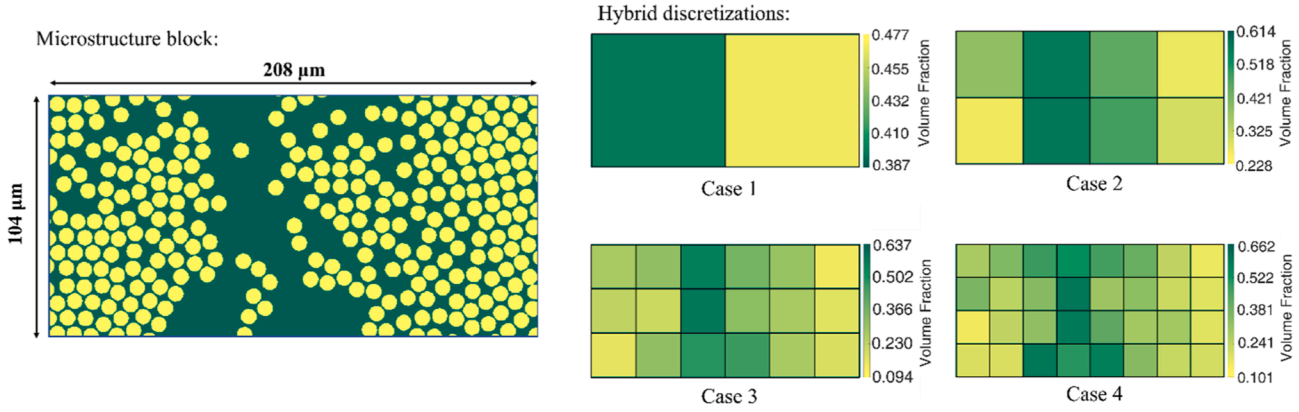

Fig. 11. Microstructure block with resin-rich uncertainty and its hybrid discretization.

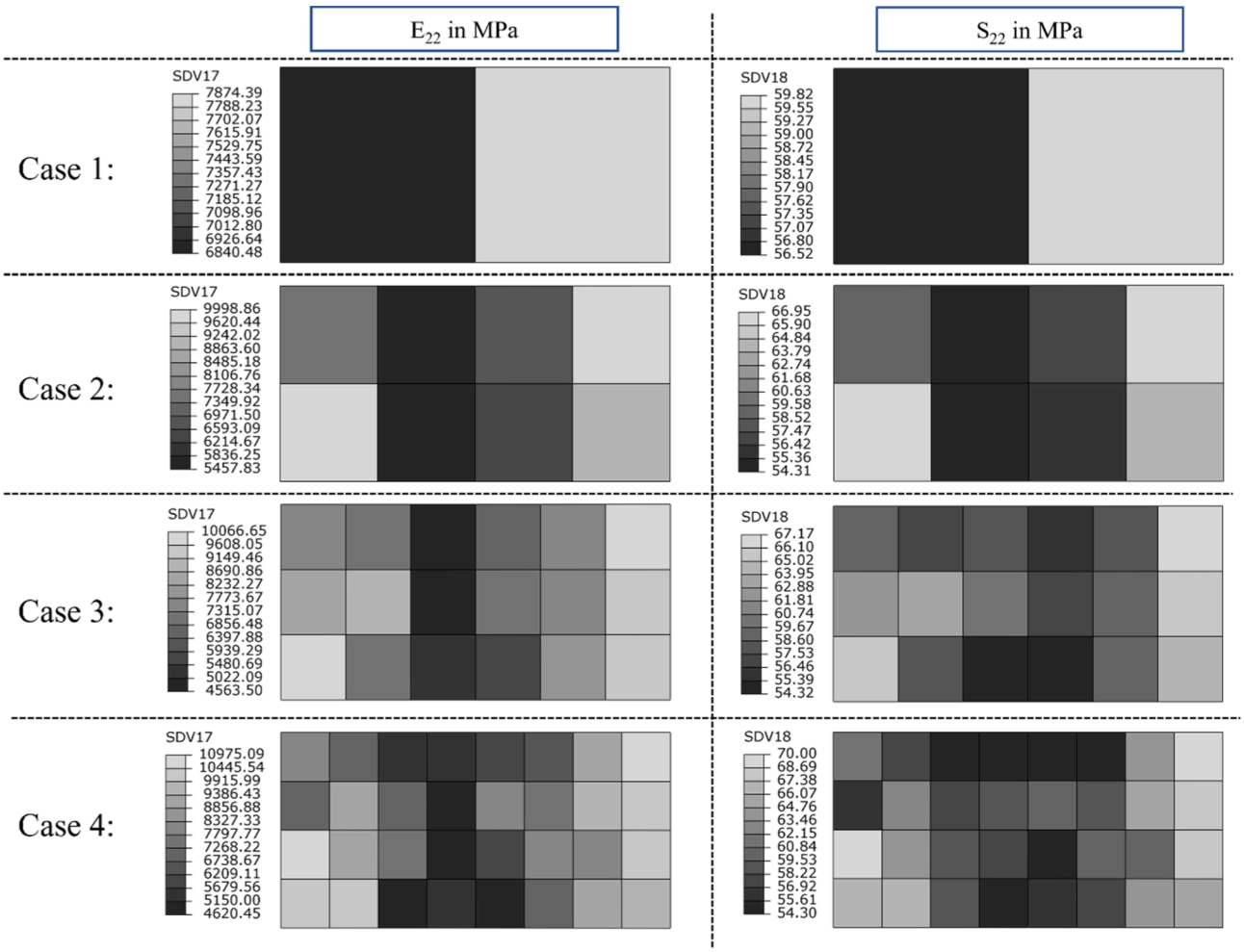

Fig. 12. Scatter of the transverse modulus and strength mechanical properties.

fraction can be observed from models with different window sizes in Fig. 8. Unlike similar studies, the window size was not considered constant for different models of this study to see its influence on the simulation results. The correlation was discussed in [13] and a window size of 70 μm was suggested for the window size while here since the windows are not distributed randomly and the simulations were not performed stochastically a further decrease of the window size was possible. For the hybrid model, the location-based information of fibre volume fraction was recorded for each microstructure and used as an input for the user-defined material model to estimate the macro scale properties in each element. Then the microstructures were subjected to pure transverse load for the prediction of effective properties.

Fig. 9-a shows the effect of fibre volume fraction on the stress–strain response of the microstructures of Fig. 8 from the micromechanical simulation. As expected, the transverse modulus increases with the increase of the volume fraction, while the failure strain decreases with the increase of the fibre volume fraction. The transverse moduli of the microstructures were also estimated by using the hybrid damage model which utilized the ROM, Chamis, and bridging with $\beta = 0.7$ formulations, see Table 4. Fig. 9-b shows the comparison of the predicted

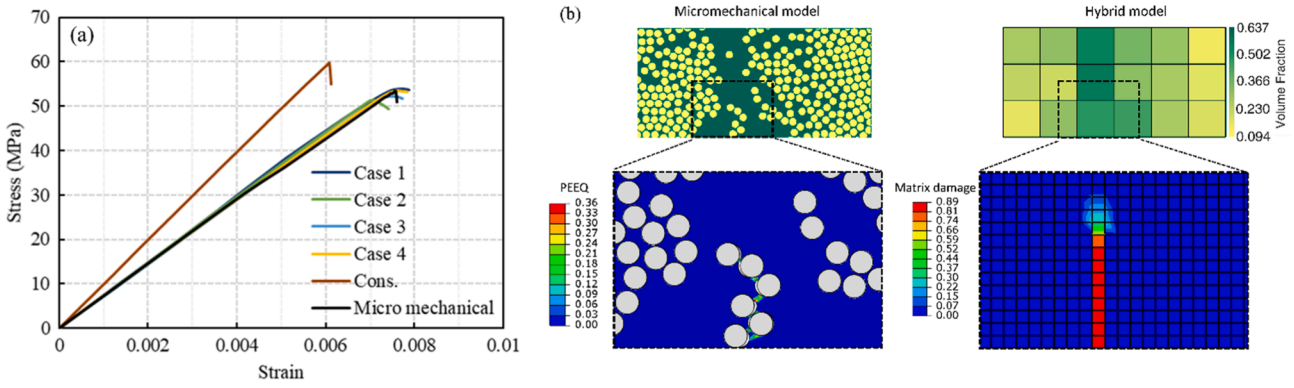

Fig. 13. (a): Comparison of the transverse stress–strain curve from the micromechanical FE simulation and hybrid damage model, (b): Comparison results of crack extension from the micromechanical and hybrid model (Case-3) at 0.7% applied strain.

transverse modulus from the micromechanical simulation and the hybrid damage model with different analytical formulations. The solid line in Fig. 9-b is the total agreement between the results of the two simulation approaches, while the band between the two dashed lines is the area of less than ± 10 %. Like in the case of single fibre RVE, the bridging formulation with $\beta = 0.7$ is the most accurate in predicting the transverse modulus of the microstructures with different volume fractions and therefore was chosen as the only equation to estimate the transverse modulus hereafter.

The investigation of the transverse strength has been performed on the microstructures in Fig. 8. In this case, the transverse strength was estimated by the Chamis, modified Chamis, and Bridging models in the hybrid damage model. In the case of fibrous composites, the significant batch-to-batch variation in the transverse strength is steered by the fibre/matrix interface properties. Normally the failure initiates at weak links between fibre and matrix and increasing the fibre volume content may demean the transverse performance of the material by introducing more physical factors such as weak links, voids, and fibre waviness [44]. Since such weak links are not considered in the micromechanical simulations of this paper, the failure is driven by the fibre/matrix interface properties which use a stress-based failure criterion for the prediction of the onset of damage. Therefore, as it can be seen from Fig. 9-a similar value of transverse strength is predicted by the micromechanical FE models of different fibre volume contents. While the transverse strength is similar for different microstructures, a remarkable difference can be observed in the failure strain of the models. Increasing the fibre volume leads to lower values of the failure strain in the microstructures. Similar results were reported in [44].

The results of the comparison between the micromechanical and hybrid damage models are shown in Fig. 10. The hybrid simulations with modified Chamis formulation were performed with different values of n_t. The dashed lines in Fig. 10-a show the band of ± 10 % error and the solid line indicates the exact prediction by the hybrid model. In this regard, the points that are closer to the solid line show more accuracy. The total aggregate error of the different formulations is compared in Fig. 10-b. Based on the comparison between the two simulation approaches, the modified Chamis semi-analytical model with $n_t = 2.5$ was chosen for the estimation of the transverse strength hereafter.

3.3. RVE with resin-rich variability

In this section, the hybrid damage model is used for the simulation of a block of CFRP microstructure with resin-rich uncertainty which is shown in Fig. 11. Four different hybrid discretization cases were considered with different window sizes which are 1 by 2, 2 by 4, 3 by 5, and 4 by 8. As mentioned in Fig. 1 the scatter of the fibre volume fraction is used as the input of the user-defined material model at the beginning of the hybrid simulation. Here the Bridging model and modified Chamis formulation were used to estimate the transverse modulus and strength, respectively. Estimation of the material properties at the beginning of the simulation leads to a scatter of material properties in different elements of the hybrid model. This scatter for the transverse modulus and transverse strength is shown in Fig. 12. Decreasing the window size led to higher variations in the scattered mechanical properties of Fig. 12.

Fig. 13-a shows the comparison of transverse stress–strain curves for the microstructure of Fig. 11 up to failure. The presence of the resin-rich zone led to a decrease in the transverse stiffness and an increase in the failure strain compared to a block of the same material with a constant volume fraction of 0.6, see the red curve (cons.) in Fig. 13. The uncertainty has decreased the transverse modulus by 25.2 % and has increased the failure strain by 27.0 %. The prediction of the stiffness from the micromechanical FE simulation is in good agreement with the hybrid model in all cases in Fig. 11. This is due to the non-stochastic scheme and the use of a microstructure image of the composite in the simulations which resulted in the diminished influence of the discretization window size. Meanwhile different results would be expected if the distribution fit of Fig. 4 would be used to perform the simulation in a stochastic manner. Therefore, by using the actual image of the microstructure and using the point-to-point map for the estimation of the mechanical properties the effect of the size of the windows on the discretization of the microstructure is mitigated. The comparison of crack extension from the micromechanical and hybrid models is presented in Fig. 13-b at 0.7 % applied strain. Both simulation approaches predict the cracks in the vicinity of the resin-rich zones which is also reported in [5], also a good correlation between the crack length and location may be observed indicating the possible capability of the novel approach in predicting the failure.

4. Conclusion

In this paper, a hierarchical hybrid micro–macro mechanical damage model was proposed for the simulation of fibrous composites. The model works based on discretising the microstructure into a grid of windows and performing image processing to identify the information on the microstructure level. Then by using analytical and semi-analytical micromechanical formulations, the material properties are estimated using a user-defined material model in Abaqus. Therefore, the model does not require the solution of the micromechanical FE simulation which makes it computationally efficient. The micromechanical step of the hybrid model used a modification of Puck failure criteria to simulate the progressive damage in composites. The model was verified by comparison with the micromechanics FE simulations with RVEs of different volume fractions.

The comparative results between different micromechanical formulations showed that the Bridging model works better for the prediction of the transverse modulus, while the modified Chamis model was chosen to estimate the transverse strength. The hybrid model was used to perform the simulation on a block of microstructure with resin-rich uncertainty and proved to be accurate in predicting the transverse response of the composite microstructure. The point-to-point mapping of the volume fraction to the estimated properties of the microstructure was shown to be an accurate method to investigate the resin-rich uncertainty and can be considered a useful tool for reducing the computation cost for such investigations which are normally performed stochastically.

5. Data availability statement

The raw/processed data required to reproduce these findings have been obtained from literature. Papers are reported in the references.

CRediT authorship contribution statement

M. Rezasefat: Conceptualization, Methodology, Software, Investigation, Validation, Visualization, Writing – original draft. **Y. Mostafavi:** Software, Resources, Investigation, Visualization. **D. Ma:** Methodology, Resources, Writing – review & editing. **A. Manes:** Conceptualization, Writing – review & editing, Supervision, Project administration, Funding acquisition.

Declaration of Competing Interest

The authors declare that they have no known competing financial interests or personal relationships that could have appeared to influence the work reported in this paper.

Data availability

Data will be made available on request.

References

[1] Sharifpour F, Montesano J, Talreja R. Assessing the effects of ply constraints on local stress states in cross-ply laminates containing manufacturing induced defects. Compos Part B Eng 2020;199:108227. https://doi.org/10.1016/J.COMPOSITESB.2020.108227.

[2] Arteiro A, Catalanotti G, Melro AR, Linde P, Camanho PP. Micro-mechanical analysis of the in situ effect in polymer composite laminates. Compos Struct 2014;116:827–40. https://doi.org/10.1016/J.COMPSTRUCT.2014.06.014.

[3] Saito H, Takeuchi H, Kimpara I. Experimental evaluation of the damage growth restraining in 90° layer of thin-ply CFRP cross-ply laminates. Adv Compos Mater 2012;21:57–66. https://doi.org/10.1163/156855112X629522.

[4] Huang ZM. A bridging model prediction of the ultimate strength of composite laminates subjected to biaxial loads. Compos Sci Technol 2004;64:395–448. https://doi.org/10.1016/S0266-3538(03)00220-3.

[5] Ahmadian H, Yang M, Soghrati S. Effect of resin-rich zones on the failure response of carbon fiber reinforced polymers. Int J Solids Struct 2020;188–189:74–87. https://doi.org/10.1016/J.IJSOLSTR.2019.10.004.

[6] Ghayoor H, Marsden CC, Hoa SV, Melro AR. Numerical analysis of resin-rich areas and their effects on failure initiation of composites. Compos Part A Appl Sci Manuf 2019;117:125–33. https://doi.org/10.1016/J.COMPOSITESA.2018.11.016.

[7] Jiang H, Cheng F, Hu Y, Ji Y, Hu X, Ren Y. Micro-mechanics modeling of compressive strength and elastic modulus enhancements in unidirectional CFRP with aramid pulp micro/nano-fiber interlays. Compos Sci Technol 2021;206:108664. https://doi.org/10.1016/J.COMPSCITECH.2021.108664.

[8] Yang L, Yan Y, Ma J, Liu B. Effects of inter-fiber spacing and thermal residual stress on transverse failure of fiber-reinforced polymer–matrix composites. Comput Mater Sci 2013;68:255–62. https://doi.org/10.1016/J.COMMATSCI.2012.09.027.

[9] Jiang H, Ren Y, Liu Z, Zhang S. Microscale finite element analysis for predicting effects of air voids on mechanical properties of single fiber bundle in composites. J Mater Sci 2019;54:1363–81. https://doi.org/10.1007/S10853-018-2928-6/FIGURES/17.

[10] Zhu F, Zhang S, Yu D, Huang F. Fiber break evolution and fatigue life prediction of CFRP with random fiber distribution. Compos Struct 2021;259:113475. https://doi.org/10.1016/J.COMPSTRUCT.2020.113475.

[11] Koley S, Mohite PM, Upadhyay CS. A micromechanical study and uncertainty quantification for effective properties of unidirectional fibre reinforced composites. Compos Struct 2019;225:111141. https://doi.org/10.1016/J.COMPSTRUCT.2019.111141.

[12] Chu Y, Sun L, Yang X, Wang J, Huang W. Multiscale simulation and theoretical prediction for the elastic properties of unidirectional fiber-reinforced polymer containing random void defects. Polym Compos 2021;42:2958–72. https://doi.org/10.1002/PC.26028.

[13] Sanei SHR, Fertig RS. Uncorrelated volume element for stochastic modeling of microstructures based on local fiber volume fraction variation. Compos Sci Technol 2015;117:191–8. https://doi.org/10.1016/J.COMPSCITECH.2015.06.010.

[14] Tao W, Zhu P, Xu C, Liu Z. Uncertainty quantification of mechanical properties for three-dimensional orthogonal woven composites. Part II: Multiscale simulation. Compos Struct 2020;235:111764. https://doi.org/10.1016/J.COMPSTRUCT.2019.111764.

[15] Ma D, Campos Amico S, Giglio M, Manes A. Effect of fibre bundle uncertainty on the tensile and shear behaviour of plain-woven composites. Compos Struct 2021;259:113440. https://doi.org/10.1016/J.COMPSTRUCT.2020.113440.

[16] Ma D, González-Jiménez Á, Giglio M, dos Santos Cougo CM, Amico SC, Manes A. Multiscale modelling approach for simulating low velocity impact tests of aramid-epoxy composite with nanofillers. Eur J Mech A Solids 2021;90:104286.

[17] Jiang H, Ren Y, Liu Z, Zhang S, Yu G. Multi-scale analysis for mechanical properties of fiber bundle and damage characteristics of 2D triaxially braided composite panel under shear loading. Thin-Walled Struct 2018;132:276–86. https://doi.org/10.1016/J.TWS.2018.08.022.

[18] Omairey SL, Dunning PD, Sriramula S. Influence of micro-scale uncertainties on the reliability of fibre-matrix composites. Compos Struct 2018;203:204–16. https://doi.org/10.1016/J.COMPSTRUCT.2018.07.026.

[19] Reuss A. Berechnung der Fließgrenze von Mischkristallen auf Grund der Plastizitätsbedingung für Einkristalle. ZAMM - J Appl Math Mech / Zeitschrift Für Angew Math Und Mech 1929;9:49–58. https://doi.org/10.1002/ZAMM.19290090104.

[20] Chamis CC, Abdi F, Garg M, Minnetyan L, Baid H, Huang D, et al. 2013 undefined. Micromechanics-based progressive failure analysis prediction for WWFE-III composite coupon test cases. JournalsSagepubCom 2013;47(20-21):2695–712.

[21] Sendeckyj GP, Wang SS, Steven Johnson W, Stinchcomb WW, Chamis CC. Mechanics of Composite Materials: Past, Present, and Future. J Compos Technol Res 1989;11(1):3.

[22] Huang ZM. Simulation of the mechanical properties of fibrous composites by the bridging micromechanics model. Compos Part A Appl Sci Manuf 2001;32:143–72. https://doi.org/10.1016/S1359-835X(00)00142-1.

[23] Huang Zming. Micromechanical prediction of ultimate strength of transversely isotropic fibrous composites. Int J Solids Struct 2001;38:4147–72. https://doi.org/10.1016/S0020-7683(00)00268-7.

[24] Puck A, Kopp J, Knops M. Guidelines for the determination of the parameters in Puck's action plane strength criterion. Compos Sci Technol 2002;62:371–8. https://doi.org/10.1016/S0266-3538(01)00202-0.

[25] Puck A, Schürmann H. Failure analysis of FRP laminates by means of physically based phenomenological models. Fail. Criteria Fibre-Reinforced-Polymer Compos., Elsevier Ltd; 2004, p. 832–76. https://doi.org/10.1016/B978-008044475-8/50028-7.

[26] Gonzalez RC, Woods RE, Eddins SL. Color image processing. Digit Image Process 2008; 3: 416–82.

[27] Fertig RS, Jensen EM. Effect of fiber volume fraction variation across multiple length scales on composite stress variation: the possibility of stochastic multiscale analysis. In: 55th AIAA/ASMe/ASCE/AHS/SC Struct. Struct. Dyn. Mater. Conf., 2014, p. 1169.

[28] Marsden C, Li C, Biernacki M, Carnegie SJ. 4-point bending fatigue testing of thin carbon-epoxy laminates. Proc. 19th Internafional Conf. Compos. Mater., 2013.

[29] Huang ZM, Liu L. Predicting strength of fibrous laminates under triaxial loads only upon independently measured constituent properties. Int J Mech Sci 2014;79:105–29. https://doi.org/10.1016/J.IJMECSCI.2013.08.010.

[30] Vignoli LL, Savi MA, Pacheco PMCL, Kalamkarov AL. Multiscale approach to predict strength of notched composite plates. Compos Struct 2020;253:112827. https://doi.org/10.1016/J.COMPSTRUCT.2020.112827.

[31] Vignoli LL, Savi MA, Pacheco PMCL, Kalamkarov AL. Micromechanical analysis of transversal strength of composite laminae. Compos Struct 2020;250:112546. https://doi.org/10.1016/J.COMPSTRUCT.2020.112546.

[32] Huang Z-M, Xin L-M. In situ strengths of matrix in a composite. Acta Mechanica Sinica 2017;33(1):120–31.

[33] Rezasefat M, Gonzalez-Jimenez A, Giglio M, Manes A. Numerical study on the dynamic progressive failure due to low-velocity repeated impacts in thin CFRP laminated composite plates. Thin-Walled Struct 2021;167:108220. https://doi.org/10.1016/j.tws.2021.108220.

[34] Rezasefat M, Gonzalez-Jimenez A, Giglio M, Manes A. An evaluation of Cuntze and Puck inter fibre failure criteria in simulation of thin CFRP plates subjected to low velocity impact. Compos Struct 2021;278:114654.

[35] Naya F, González C, Lopes CS, Van der Veen S, Pons F. Computational micromechanics of the transverse and shear behavior of unidirectional fiber reinforced polymers including environmental effects. Compos Part A Appl Sci Manuf 2017;92:146–57. https://doi.org/10.1016/J.COMPOSITESA.2016.06.018.

[36] Vaughan TJ, McCarthy CT. Micromechanical modelling of the transverse damage behaviour in fibre reinforced composites. Compos Sci Technol 2011;71:388–96. https://doi.org/10.1016/J.COMPSCITECH.2010.12.006.

[37] Sharma A, Daggumati S, Gupta A, Van Paepegem W. On the prediction of the bi-axial failure envelope of a UD CFRP composite lamina using computational micromechanics: Effect of microscale parameters on macroscale stress–strain behavior. Compos Struct 2020;251:112605. https://doi.org/10.1016/J.COMPSTRUCT.2020.112605.

[38] 4-Point bending fatigue of thin carbon-epoxy laminates, - Google Scholar n.d. https://scholar.google.com/scholar?q=4-Point bending fatigue of thin carbon-epoxy laminates, (accessed August 16, 2021).

[39] Kaddour A, Hinton M, Smith P, Li S. Mechanical properties and details of composite laminates for the test cases used in the third world-wide failure exercise: Http://DxDoiOrg/101177/0021998313499477 2013;47:2427–42. https://doi.org/10.1177/0021998313499477.

[40] Chevalier J, Camanho PP, Lani F, Pardoen T. Multi-scale characterization and modelling of the transverse compression response of unidirectional carbon fiber reinforced epoxy. Compos Struct 2019;209:160–76. https://doi.org/10.1016/J.COMPSTRUCT.2018.10.076.

[41] Herráez M, Mora D, Naya F, Lopes CS, González C, Llorca J. Transverse cracking of cross-ply laminates: A computational micromechanics perspective. Compos Sci Technol 2015;110:196–204. https://doi.org/10.1016/J.COMPSCITECH.2015.02.008.

[42] Benzeggagh ML, Kenane M. Measurement of mixed-mode delamination fracture toughness of unidirectional glass/epoxy composites with mixed-mode bending apparatus. Compos Sci Technol 1996;56(4):439–49.

[43] Hinton MJ, Kaddour AS, Soden PD. Failure Criteria in Fibre-Reinforced-Polymer Composites. Fail Criteria Fibre-Reinforced-Polymer Compos 2004:1–1255. https://doi.org/10.1016/B978-0-080-44475-8.X5000-8.

[44] Hetrick DR, Sanei SHR, Bakis CE, Ashour O. Evaluating the effect of variable fiber content on mechanical properties of additively manufactured continuous carbon fiber composites: Https://DoiOrg/101177/0731684420963217 2020;40:365–77. https://doi.org/10.1177/0731684420963217.